GPPS | JOURNAL

JOURNAL OF THE GLOBAL POWER AND PROPULSION SOCIETY
journal.gpps.global

Crosswind aerodynamics of low pressure ratio fans

Original article

Article history:
Submission date: 6 November 2024
Acceptance date: 1 June 2025
Publication date: 25 August 2025

***Correspondence:**
CH: cah1003@cam.ac.uk

Peer review:
Single blind

Keywords:
axial fan aerodynamics; computational fluid dynamics; inlet distortion; installation aerodynamics

Citation:
Castillo Pardo A., Gunn E., Williams T. S., Hall C., Brandvik T., and Baralon S. (2025). Crosswind aerodynamics of low pressure ratio fans. Journal of the Global Power and Propulsion Society. 9: 143–159.
https://doi.org/10.33737/jgpps/205782

Alejandro Castillo Pardo[1], Ewan Gunn[2], Tim S. Williams[1], Cesare Hall[1,*], Tobias Brandvik[2], Stephane Baralon[3]

[1]*Whittle Laboratory, University of Cambridge, 1 JJ Thomson Ave, Cambridge CB3 0DY, UK*
[2]*Turbostream Ltd., 3 Charles Babbage Rd, Cambridge CB3 0GT, UK*
[3]*Rolls-Royce plc, Moor Lane, Derby, DE24 9HY, UK*

Abstract

Ultra-high bypass ratio (UHBPR) turbofans offer significant reductions in fuel burn and pollutant emissions due to their higher propulsive efficiency. To minimise drag and weight penalties with larger fan diameters, shorter and slimmer intakes are used. Compact intakes pose a risk of delivering highly distorted flow into the fan when operating at high power in strong crosswind. The fan-distortion interaction can degrade the thrust delivered by the engine, jeopardise the stable operability and threaten the mechanical integrity of the fan. This paper aims to understand the impact of crosswind direction on the aerodynamics of a low pressure ratio fan with both a conventional and a short intake. A fully coupled numerical model of the fan, intake and external flow-field is used to quantify how crosswind direction and intake length impact the loss generation and work through the fan. For crosswind from the left (looking into the engine) the ground vortex is co-rotating relative to the fan direction. This causes co-swirl at the fan tip at entry to the windward lip separation leading to reduced incidence and fan work. In contrast, crosswind from the right causes counter-swirl towards the fan tip as it leaves the separated region, leading to higher work and large corner separations extending down the span. A shorter intake length has a more closely coupled fan and intake lip, which tends to suppress the extent of the windward lip separation, but increases the swirl variations at the casing. This leads to reduced rotor losses for crosswind from the right but increased loss for crosswind from the left. Overall, for a short intake, the fan work is found to be around 6% higher for crosswind from the right relative to crosswind from the left. Despite the large levels of distortion in extreme crosswind, the prototype fan demonstrates in all cases it can operate stably without a significant drop in performance.

Introduction

Shortened civil aero engine intakes could lead to fuel burn savings by reducing the weight and drag of the nacelle (Hoheisel, 1997). This effect is especially important given the ongoing trend towards lower pressure ratio, larger engine fans which increase the nacelle diameter required for a given engine thrust. However, short intakes deliver a more distorted flow to the fan, which can influence its performance especially at off-design conditions.

Crosswind is here defined as the operating condition where the free-stream vector is parallel to the ground plane and normal to the engine axis. Figure 1 presents a sketch showing a section of the fan and intake system for a plane parallel to the ground that passes through the engine

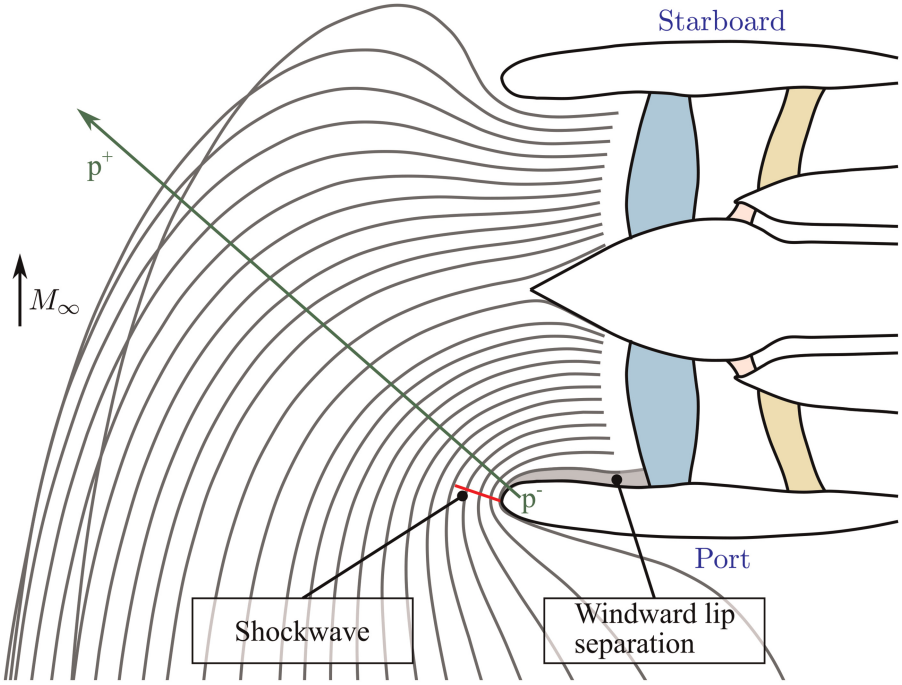

Figure 1. Top view of engine section symmetry plane and ingested streamlines for crosswind from the right.

centreline. The figure shows ingested streamlines that pass through this plane just upstream of the fan for a strong crosswind from the right. This operating condition is characterised by the following features:

- The captured streamtube area far upstream of the engine, $A_1 = \dot{m}/\rho_1 V_1$, is much greater than the highlight area A_{hi}. The ratio of these areas, referred to as mass flow capture ratio $MFCR = A_1/A_{hi}$, increases for crosswind when combined with the fan operating at high power.
- As the intake aligns the captured streamtube with the engine, a region of high streamline curvature appears near the intake windward leading edge. The curvature diminishes with distance from the leading edge, resulting in the static pressure gradient shown in Figure 1.
- At high mass flow conditions, the streamline curvature around the windward lip creates a patch of supersonic flow, which can terminate in a shockwave and separate the boundary layer.
- The intake diffuser imposes an adverse pressure gradient downstream of the intake throat. This gradient can separate the boundary layer from the windward lip or act to prevent reattachment if the boundary layer has already been separated upstream by a shock.
- A short intake cannot fully turn and align a strong crosswind with the engine centreline, leading to angular distortion at the fan face.

The above is a 2D interpretation of the flow field. In reality, crosswind is a highly 3D phenomenon. The captured streamtube, which is large enough to intersect with the ground plane, is turned downwards as well as horizontally. A top-to-bottom asymmetry is present due to the restrictive nature of the ground plane. Murphy and MacManus (2011), De Siervi et al. (1982), and Trapp and da Motta Girardi (2010) show that shear and vorticity are generated by the turning of the streamtube over the nacelle surface and ground plane. This vorticity creates the ground vortex (GV) ingested by the engine.

For a given fan rotational direction, the ground vortex can be either co-rotating or counter-rotating relative to the fan. The sense of rotation of the ground vortex is determined by the crosswind direction. The ingestion of a counter-rotating ground vortex has been linked to increased fan pressure ratio and reduced isentropic efficiency, whilst the opposite trend holds for a co-rotating vortex (Castillo Pardo et al., 2014). The interaction of the fan with tip-low total pressure distortion has been found to rise the work and pressure rise (Allen et al., 2021). However, both studies prescribed the distortion and no upstream effect of the fan on the distortion generation was accounted for.

The remainder of this paper is structured as follows. We first introduce the fully coupled numerical model of the low pressure compressor system of the prototype UHBPR turbofan. We then describe the different test cases that are used, focusing on two different intake designs and both crosswind directions. The resulting intake flow

field is then analysed in detail, emphasising the interaction between the nacelle separation, ground vortex ingestion and the resulting distortion present at the fan face. We then consider the fan stage flow field for all cases, showing that the fan response changes significantly for left and right crosswind and for each intake design. Finally, the implications of crosswind operation on overall performance and loss are quantified for each part of the low pressure compressor system.

Test cases

Figure 2 presents a schematic of the numerical domain used for the coupled crosswind simulations. The fan and installation system comprises: (i) a conventional intake with $L/D_F \approx 0.54$ or a short intake with $L/D_F \approx 0.34$, where length is measured from the fan leading edge, (ii) complete fan system with rotor, OGV and ESS, (iii) cylindrical bypass exhaust duct and nozzle. Both intake designs are three-dimensional, non-axisymmetric, drooped designs. The turbomachinery is representative of a future low-pressure ratio ultra-high bypass ratio fan stage. A large freestream domain was used with the turbofan engine in the centre. Freestream boundaries were set at 17 fan diameters, D_F, away from the fan in all directions, except for a viscous ground plane located underneath the engine. The boundary distance from the fan was chosen so that the engine static pressure field had negligible influence on the boundary flow. The external fan nacelle geometry was extended downstream as a cylinder to the freestream boundary location. An inviscid boundary condition was applied to the cylinder starting from the point where the fan exhaust would be located in a real installation, so that the viscous effect of the real nacelle is accounted for but the extension has minimal influence on the flow field. The ground plane was set such that the distance from the intake highlight to the ground plane at bottom dead centre was $h/D_F = 0.39$ for both intakes. This distance is expected to be representative of a typical value for a future ultra-high bypass

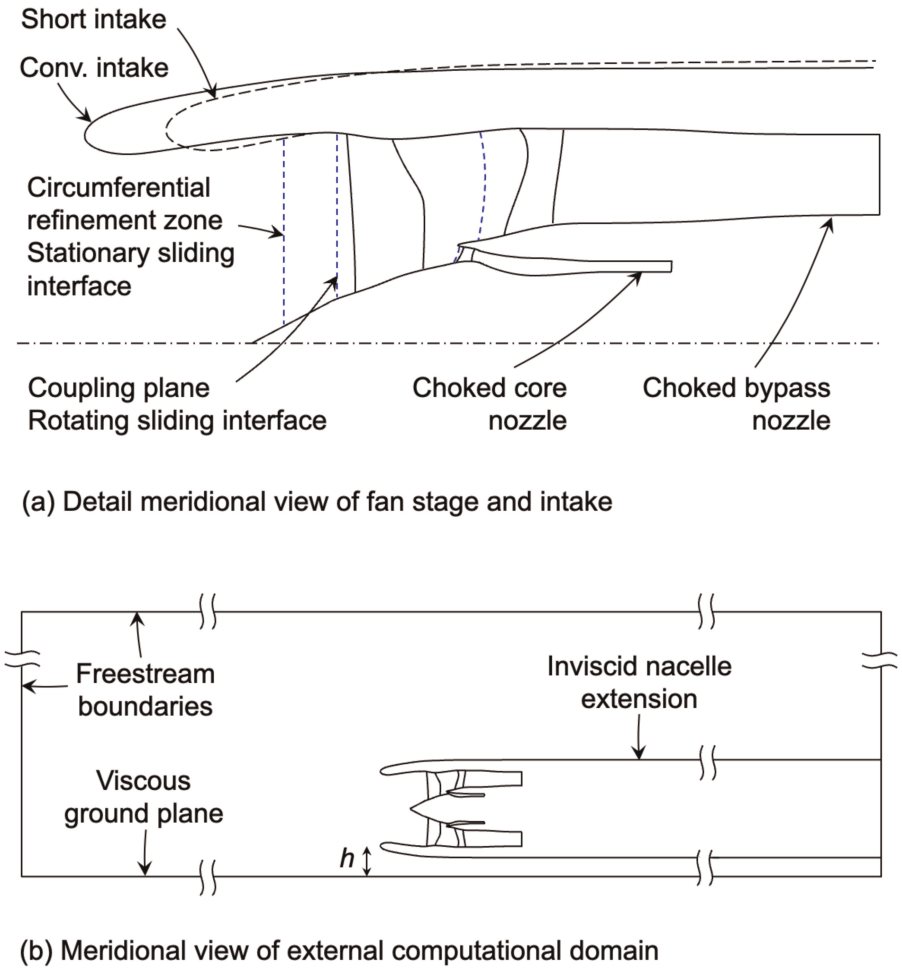

Figure 2. Meridional view of the computational domain.

Table 1. Fan and intake design parameters.

Fan stage design pressure ratio	1.4
Rotor inlet tip M_{rel}	>1
Rotor tip Reynolds number at cruise	5.5×10^6
Rotor inlet hub/tip radius ratio	0.25
Intake length: L/D_F	Conv.: 0.54 Short: 0.34
Cruise intake lip Reynolds number	2×10^6

turbofan installation. The relevant fan and intake design parameters are summarised in Table 1. All components were designed by Rolls-Royce plc.

Table 2 presents a summary of the main crosswind operating conditions studied in this paper. Two different crosswind angles are analysed: 90° and −90°, which correspond to crosswind blowing directly from the right and left of the engine, respectively. A crosswind speed of 35.0 kt was chosen. This represents a realistic crosswind condition where an aircraft would be expected to operate, but also represents a strong enough crosswind to produce a separated intake flow so that the results capture the effect of a strong fan-intake interaction. Comparisons are also made to the fan performance at a reference non-crosswind operating condition. This is defined as a coupled simulation at the same non-dimensional condition but without the presence of a ground plane and where the freestream flow is at 0° i.e. a direct headwind. This means that the reference case has negligible fan inlet distortion and represents an idealised flow field at this operating condition.

Computational methods

Full annulus, unsteady simulations were carried out using the GPU-accelerated Reynolds-averaged Navier Stokes solver `Turbostream` (Brandvik and Pullan, 2011). Boundary layers were modelled as fully turbulent and the one-equation Spalart-Allmaras (SA) turbulence model (Spalart and Allmaras, 1992) was used for all simulations along with adaptive wall functions on all solid walls. The helicity-corrected version of the SA model (Liu et al., 2011) was applied, based on previous work showing its suitability for predicting separated and stalled flows in fans (Lee et al., 2018; Kim et al., 2019). Jameson's dual time stepping method (Jameson, 1991) was used to march the simulation in time with 2880 time steps per revolution. This temporal resolution has been used and validated successfully in `Turbostream` for the prediction of stall inception in low pressure ratio fans (Kim et al., 2019).

The boundary conditions are defined at sea level conditions, representative of a beginning of runway condition. Freestream static properties p_1, T_1, Mach number M_1 and yaw angle β_1 are specified at the boundary of the

Table 2. Test case operating conditions.

Altitude (ft)	0.0
Crosswind speed	35.0 kt ($M = 0.054$)
Crosswind angle	$\pm 90.0°$
Fan rotational speed (%)	100.0
Fan operating point	Intersection with sea level static working line

external domain to define the crosswind flow, and at a given boundary point the flow can enter or exit the domain as required depending on the local conditions. The boundary layer of the wind approaching the engine is allowed to self-develop over the ground, which is modelled as a non-slip wall. This is valid due to the negligible link between the boundary layer properties and the ground vortex characteristics (De Siervi et al., 1982; Murphy and MacManus, 2011).

Within the fan stage, a long converging choked nozzle is used to set the core exit boundary condition. The area of the core nozzle is adjusted to obtain the mass flow at the reference operating condition, and it is later held constant for crosswind, fixing the non-dimensional outlet core mass flow. A converging choked nozzle is also used to set the bypass exit boundary condition. The bypass nozzle area for the simulations was determined by first running a single-passage, steady characteristic where the bypass nozzle area was varied to control the fan operating point. This characteristic intersects the sea level static fan working line at a particular nozzle area. This area was then applied to the simulations. This mimics the behaviour of a choked engine nozzle. When crosswind is introduced, the fan performance changes compared to the design point and its operating point moves along an operating line defined by a constant non-dimensional exit flow function. In reality, the nozzle of a low pressure ratio fan at a sea level static condition is likely to be unchoked. In this case, the fan operating point would move along a different operating line to that shown here, determined by the nozzle geometry and far field static pressure. This line would have a lower slope and bring the fan closer to its stability limit. The larger the deviation from the design point, the larger the difference between choked and unchoked conditions. The results shown here represent small excursions from the design condition, despite the large distortion, so this behaviour would not affect the findings shown. The unchoking behaviour of a real nozzle could be modelled by including the rear nacelle and exhaust geometry directly in the simulation.

Multi-block structured grids were generated for the fan stage and intake domains using `NUMECA Autogrid` (NUMECA International, 2016) and `Pointwise` (Pointwise Inc, 2023), respectively. A y^+ of approximately 3 was attained at the intake and turbomachinery walls. The intake, exhaust and free-stream mesh contains 50×10^6 cells, with approximately 50 near-wall layers on the intake, and the full annulus fan stage mesh contains 106×10^6 with approximately 30 near-wall layers around the blades and on the endwalls. Sliding planes are used to connect rotating and stationary domains.

A mesh independence study of the external domain was performed with the procedure proposed by Celik et al. (2008). An isolated engine installation subjected to 35 kt of crosswind was assumed, with uniform and constant pressure boundary condition at the fan face. Three levels of mesh refinement were studied: level 1, 2 and 3. These correspond to 13.5×10^6, 27.1×10^6 and 55.1×10^6 cells, respectively. The Grid Convergence Index (CGI) was used to assess the impact of spatial discretisation on the predicted fan face mass flow rate. Level 2 mesh was sufficiently mesh independent with a GCI compared to level 3 mesh of 0.25% when estimated for the fan face mass flow. The mesh density used for the fan stage is consistent with the level used by Williams et al. (2020), which was proved appropriate for a similar application.

A subscale version of a similar transonic fan stage was experimentally tested to validate the numerical model. Single-passage steady-state simulations of an isolated fan stage were performed for this validation. The simplified domain comprises a fan blade connected to a long straight intake duct and axisymmetric ESS and OGV vanes attached to their respective choked long nozzles. Figure 3 shows close agreement between numerical predictions and rig measurements of the design speedline.

Intake flow field

The flow under crosswind has two additional complicating factors compared with regular operation. Firstly, the intake droop plane is normal to the direction of the freestream flow. Secondly, the intake and fan are influenced by the presence of the ground, which modifies the potential field and leads to ingestion of a ground vortex. Some of the resulting effects are sketched in Figure 4.

The droop and freestream flow directions are orthogonal, creating two secondary flow components. The centripetal pressure gradient created as the flow is turned into the intake leads to low static pressure and a mass flow increase on the windward side. As the flow returns to a more uniform mass flow distribution, it migrates downwind across the annulus. The fan amplifies this effect. However, this effect acts in opposition to the fan's tendency to drive flow towards the separated area on the upwind side. This is shown by the opposing blue and red arrows. The intake droop also creates a tendency for flow to migrate upwards, generating a different secondary flow component under crosswind.

Both of these flow features can create co-swirl and counter-swirl in different locations relative to the intake flow separation depending on the freestream and fan rotational directions. The potential for different freestream

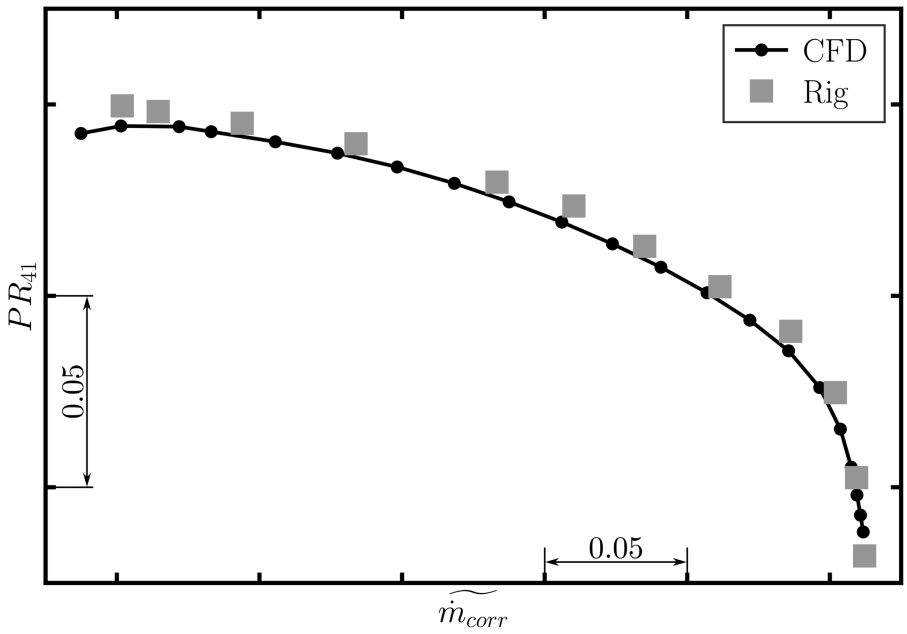

Figure 3. Design speedline comparison of CFD predictions with experimental measurements of a fan stage in clean flow. The results are shown for a fan stage that is similar to the one used for the current work.

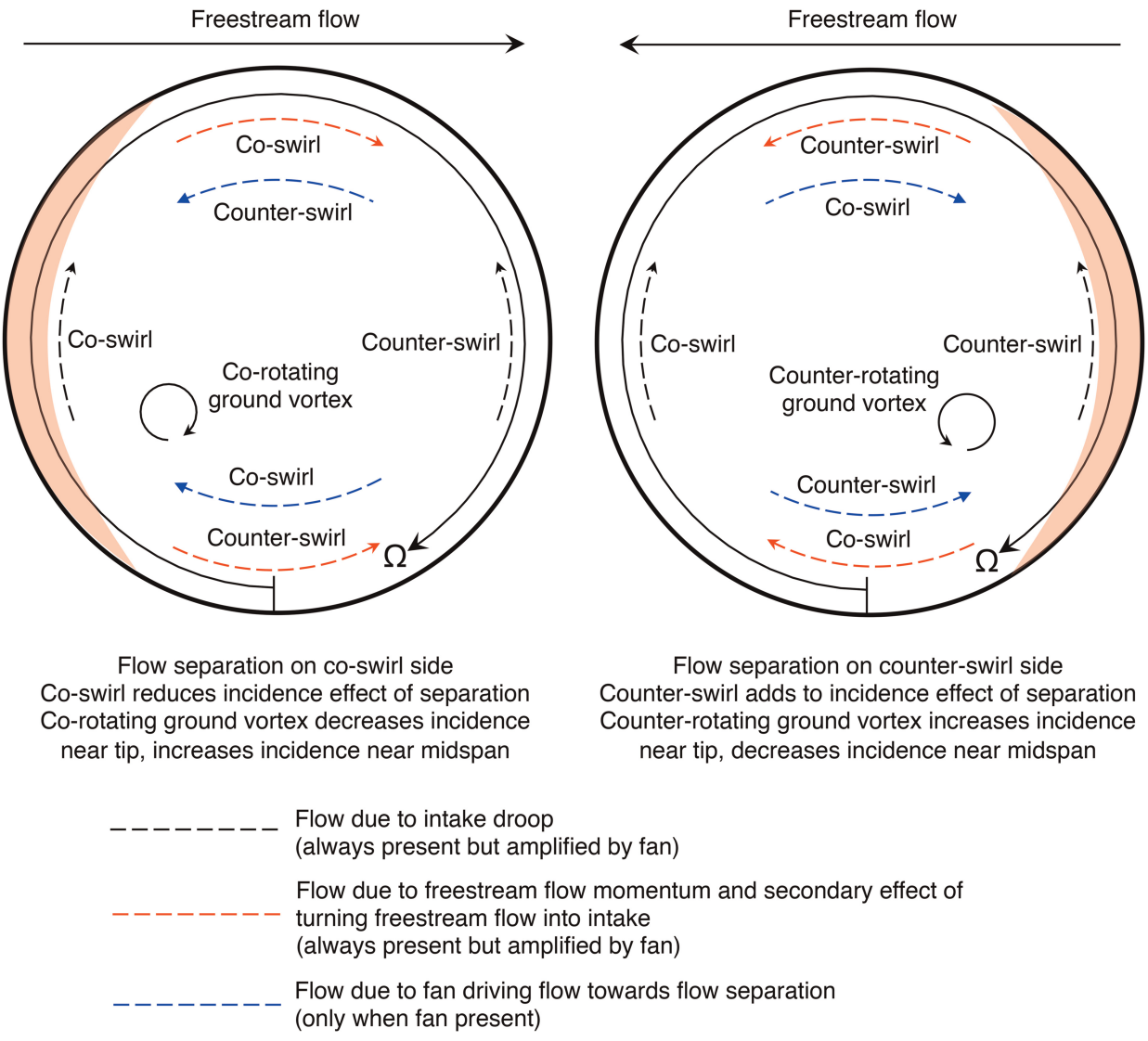

Figure 4. Schematic of the fan inlet flow field with crosswind, viewed from front looking aft.

and fan rotational directions also creates two possible senses of rotation of the ground vortex relative to the fan. The fan response to crosswind is therefore highly asymmetrical. The results presented here are shown with the fan rotating clockwise in all cases and the freestream flow is either from the left or right, as shown in Figure 4. These effects also lead to spanwise flows, which have been shown to be important at high angle of attack operating conditions (Mohankumar et al., 2021). In the present work, the freestream component of momentum is lower and the dominant effects were found to be explained by the way that these flow features superimpose to create non-uniform inlet axial velocity and swirl patterns.

Prior to running the simulations it is not obvious how these effects will combine or what the final flow field will look like. It will depend on the detailed balance of the freestream flow speed, intake design and fan design. This creates an additional reliance on the CFD to make the right prediction and is likely to complicate the challenge of designing the system for this flow field.

Figure 5 shows top-down views of the time-averaged intake flow field under crosswind. Figure 6 shows corresponding fan inlet axial mass flux distributions. The streamlines show that the fan captures flow from well round the outside of the engine cowl. This leads to higher streamline curvature and acceleration around the upwind lip compared with other flight conditions such as high angle of attack operation. In all 4 high mass flow cases considered here, a shock wave sits on the highlight around the upwind side of the intake, which separates the boundary layer immediately downstream.

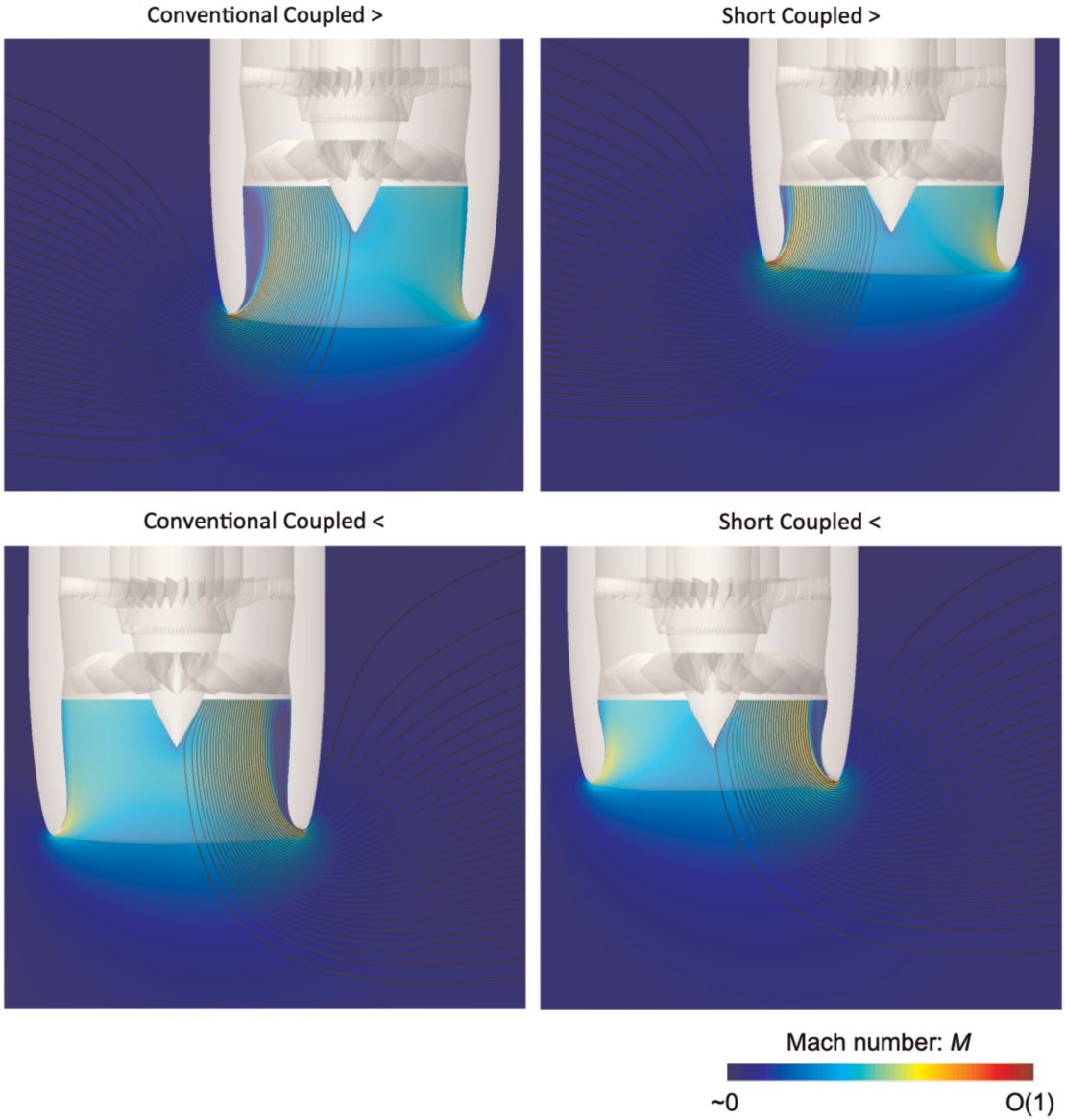

Figure 5. Contours of time-averaged Mach number and streamlines on a cut through the thickest part of the intake flow separation for coupled fan-intake operation under crosswind.

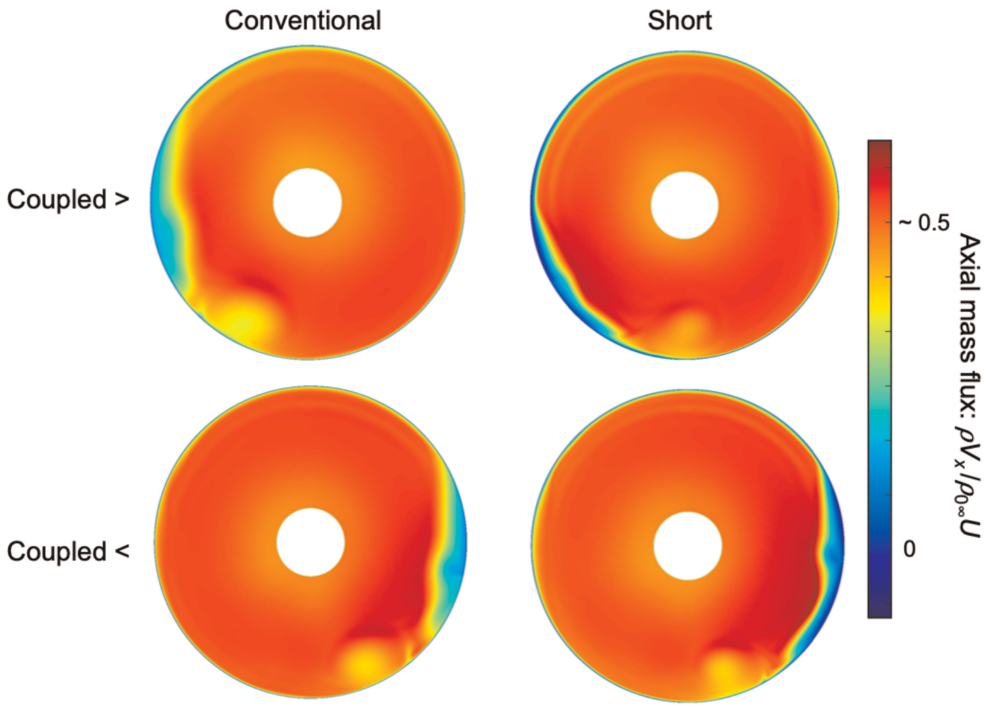

Figure 6. Contours of axial mass flux at fan inlet for coupled unsteady calculations under crosswind.

For both conventional and short intakes, and both freestream directions, the overall streamline pattern and initial location of the separation is similar. However, the downstream development of the separation differs because of the change in proximity to the fan pressure field with intake length and due to the relationship between the separation, potential field and fan rotation.

In the conventional intake, the separation grows to a larger spanwise height than that in the short intake, but the fan causes reattachment before the flow reaches the leading edge. This is shown by positive axial mass flux in Figure 6. The influence of the fan means the separation stays at a smaller size in the short intake, but the steeper diffuser angle prevents full reattachment. There is still reversed axial flow just upstream of the fan.

The ground vortex appears as a region of slightly reduced mass flux, but it is not as low as the intake separation. Figure 7 shows that the origin of the ground vortex is similar for both flow directions and both intakes. This can be explained by the fact that the separation point on the ground is relatively far away from the fan in all cases, of the order of one fan diameter. The separation is therefore driven by the bulk suction from the engine, which at this distance will be determined mainly by the 1D fan operating point alone rather than the detailed fan flow field. These results suggest the origin of the ground vortex is relatively unaffected by flow direction and intake length. Previous findings on the ground vortex in the literature should be equally applicable to short intake designs. In particular it will be shown below that the direction of the vortex is important for the fan performance.

Fan inlet flow field

Figures 8 and 9 show the time-averaged fan inlet Mach number and swirl angle distributions. Figure 10 shows the resulting fan inlet incidence for the crosswind cases relative to operation in clean flow on the working line at the same fan speed. The dominant long length scale effect is for a general trend of high Mach number on the upwind side of annulus relative to the downwind side. This is exacerbated by acceleration around the blocked area of the flow separation. There is an additional, but smaller, trend of high Mach number at the bottom of the annulus due to the droop.

Below the separations there are large regions of strong co-swirl or counter-swirl at the casing. The flow direction in these regions is against the freestream direction. They are primarily caused by the local rotation of the ground vortex, which tends to be ingested near the upwind separation location. This effect occurs with a similar intensity in both intake lengths, consistent with the fact that even in a short intake, the fan is relatively far removed from the source of the ground vortex so does not influence its creation or angular momentum. These casing swirl regions are also partly caused by the redistribution of flow towards the separated area.

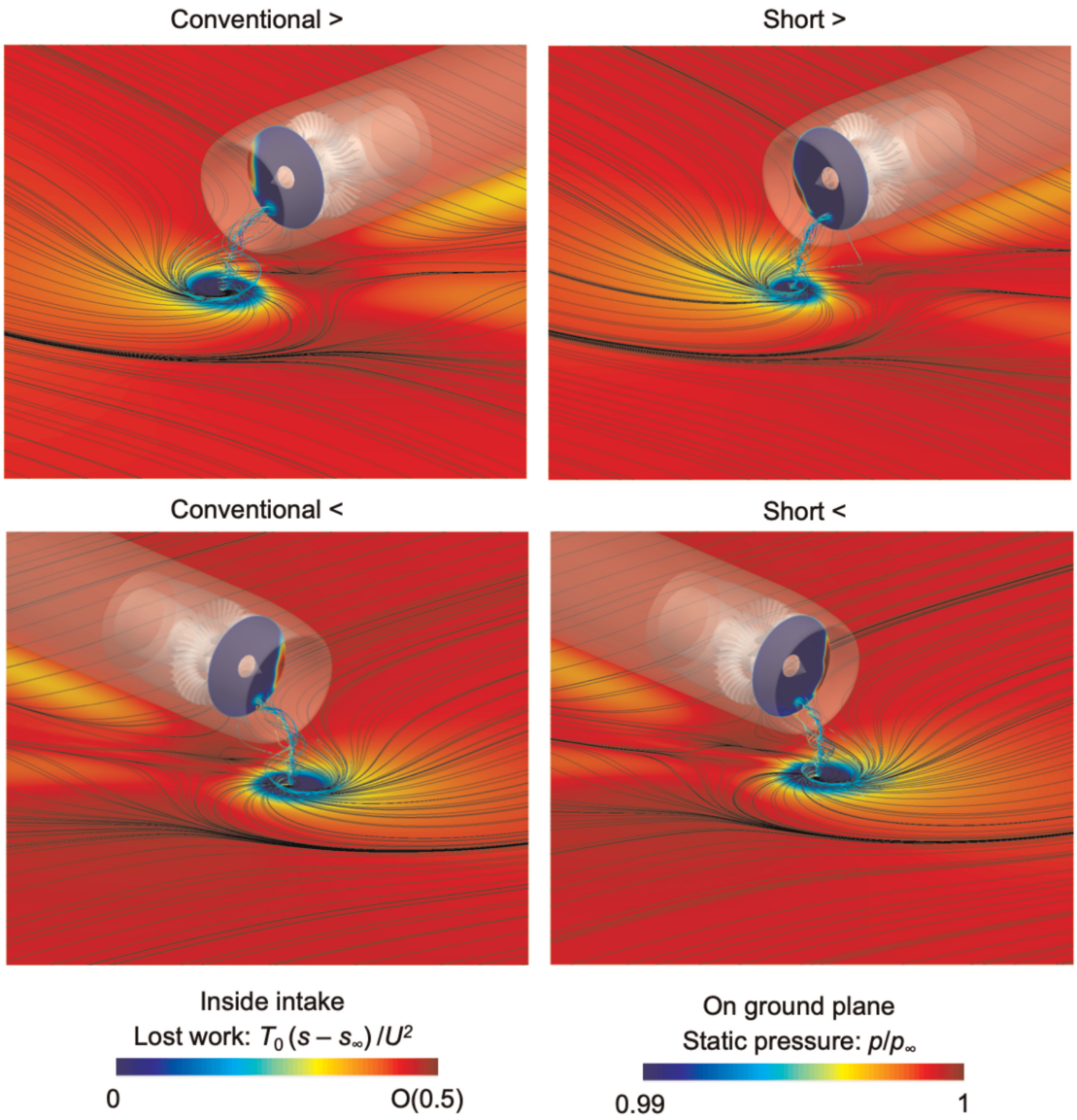

Figure 7. Contours of time-averaged lost work (inside the intake), static pressure (on the ground), and ground surface and ground vortex streamlines for coupled fan-intake operation under crosswind.

This can be seen by the presence of opposing, but significantly smaller, mirrored regions above the separation.

At around midspan the ground vortex rotation creates a region of swirl in the opposite sense to that above. This is a smaller length scale effect than the bulk flow distortion but still affects the flow over the full blade height and a width of several blade passages.

When the separation is on the right side of the annulus, it coincides with counter-swirl created by the droop (discussed below). It also coincides with an area of counter- swirl from the ground vortex. All three effects tend to increase the fan suction. For a left side separation, the suction effect imparted to the separation is moderated by co- swirl from the droop and ground vortex. The upstream acceleration effect is therefore stronger for a right-side separation than a left-side one, so the strength of the fan coupling effect depends on the freestream flow direction.

An additional, longer length scale component of swirl affects the flow away from the separation and ground vortex. The flow in the bottom half of the annulus is dominated by the ground vortex, so this additional effect is only noticeable in the upper half.

As a rough guideline, the long length scale swirl effect leads to co-swirl in the upper annulus half for free-stream flow from the left and vice-versa. Independently of the freestream direction, the droop creates counter-swirl on the right side and co-swirl on the left side. However, the effects are asymmetrical under a change in free-stream direction. They are driven by the balance between opposing effects in Figure 4 and altered by the response from the fan and location of the separation.

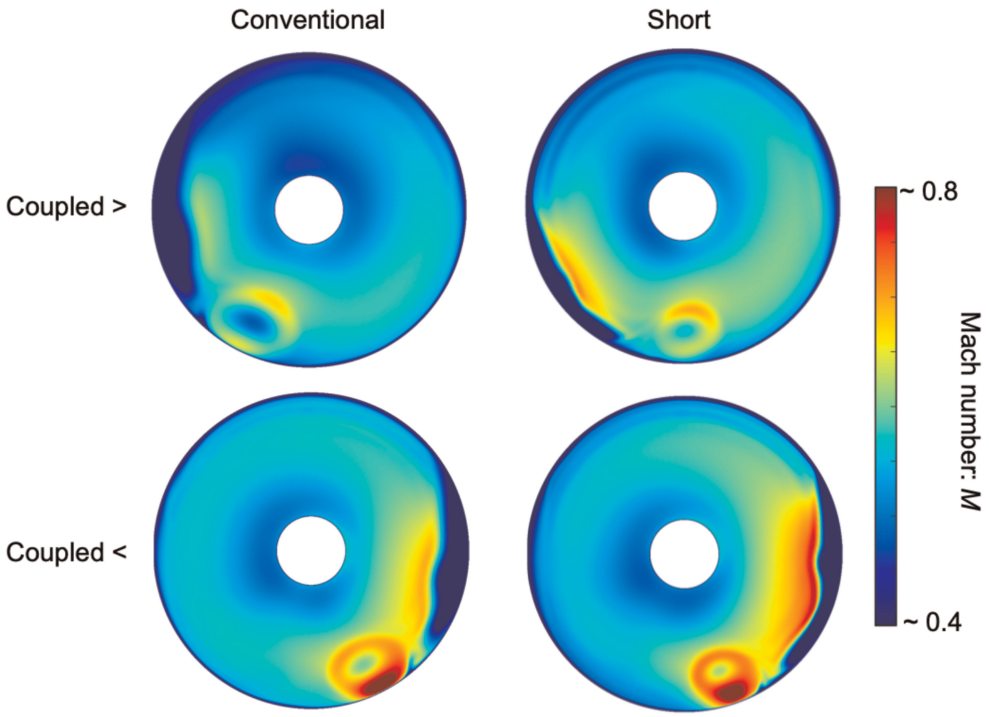

Figure 8. Contours of time-averaged Mach number at fan inlet for coupled unsteady calculations under crosswind.

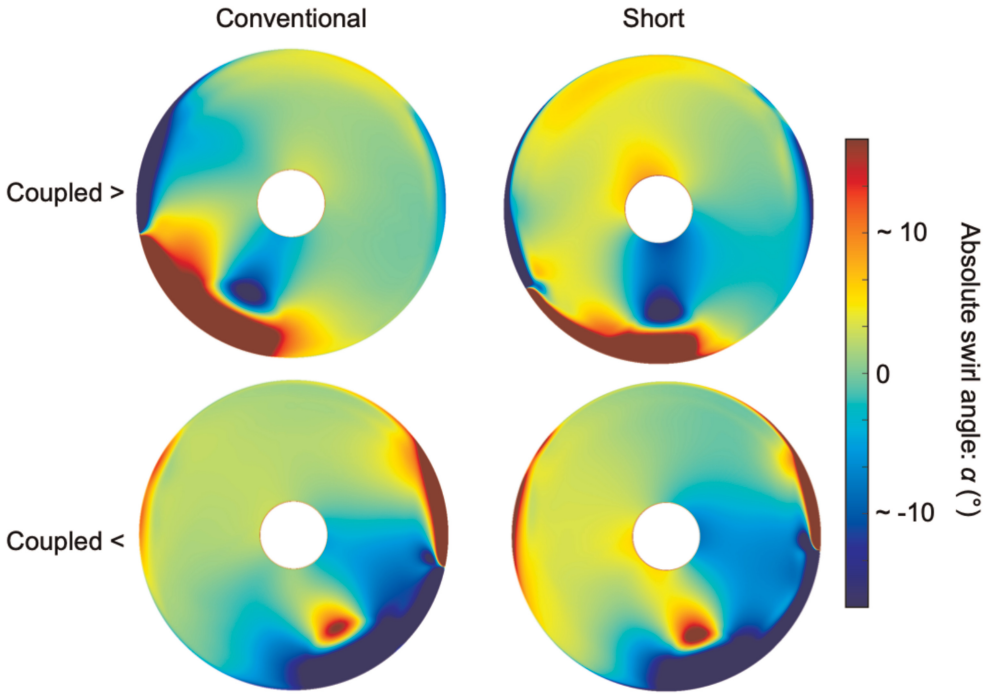

Figure 9. Contours of time-averaged absolute swirl angle at fan inlet for coupled unsteady calculations under crosswind.

The above effects are all reflected in the fan inlet incidence distributions in Figure 10. These plots show a peak-to-peak incidence fluctuation of 30° across the ground vortex and up to 25° in the separation. Although the short intake separations cover a smaller region of space than those in the conventional intake, the lower axial velocity means they create a higher incidence onto the fan.

The combination of the ground vortex, separation and 3D intake shape creates complex 3D flow distributions near the casing. Note the large incidence variations at around 85% span. These are due to the additional

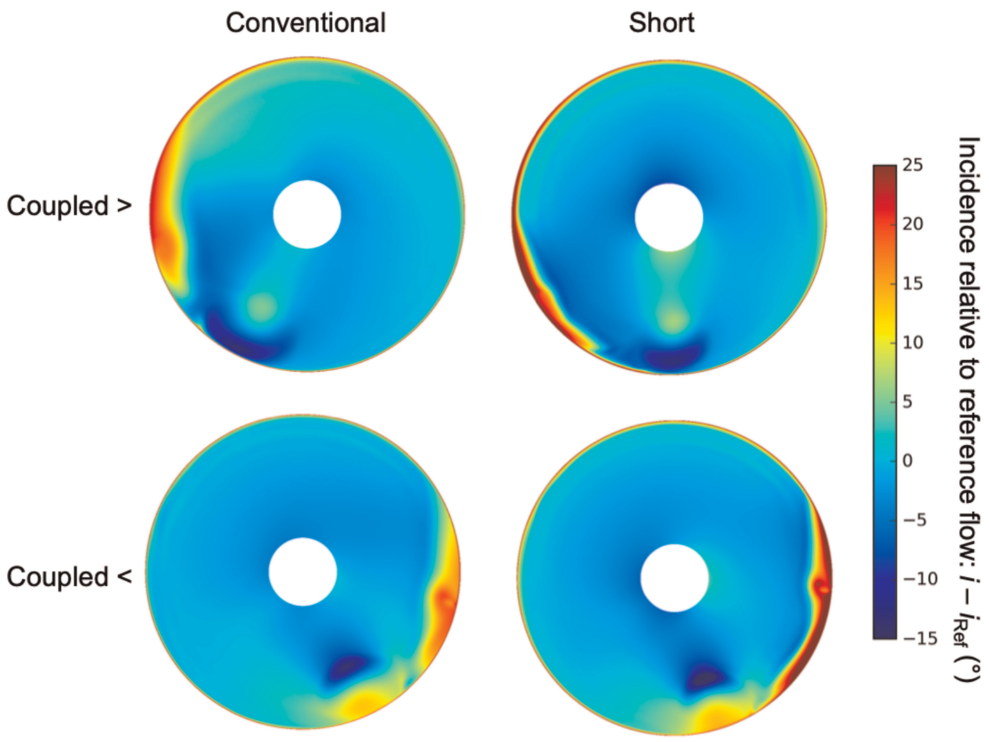

Figure 10. Contours of incidence at fan inlet relative to clean fan-alone flow field for coupled unsteady calculations under crosswind.

secondary flow components in Figure 4 combined with the ground vortex. The superposition gives different results for the different freestream directions. The combination of counter-swirl from the ground vortex and low axial velocity from the separation gives very high relative Mach number and incidence near the casing for flow from the right. For flow from the left, the combination is such that the flow is only just supersonic. This helps to explain why flow from the right leads to significantly higher fan loss, as will be shown below.

Fan stage flow field

Figures 11 and 12 show the instantaneous and time-averaged rotor and stator exit flow fields respectively. In all cases the intake flow separation creates further flow separations around the tip of the rotor blades immediately downstream. The details change depending on both intake length and freestream flow direction and the discussion below is divided by direction.

Flow from the left

For a left-side separation the main set of rotor tip separations is larger in the conventional intake. This is despite the fact that the flow reattaches before reaching the fan for the conventional intake, but remains separated in the short intake. One of the key reasons for this is that the short intake leads to stronger co-swirl in the upper half of the annulus (Figure 9). This creates a region of negative incidence (Figure 10), reducing the turning required in the rotor immediately after it leaves the separated region. The rotor blade flow is quickly "cleaned up" and reattached after leaving the intake separation, in contrast to the conventional intake where separations persist around the upper annulus.

The intake separation in the conventional intake also occupies a larger fraction of the blade height, causing large corner separations in the rotor. In the short intake the rotor flow does not form full corner separations. Instead there are distinct patterns of separated casing flow (which in fact is the intake separation itself convecting through the rotor, not a new separation in the rotor) and smaller, two-dimensional separations further down the rotor span.

For flow from the left, the ground vortex is distinct from the intake flow separation so its effect on the fan can be seen clearly. It creates counter-swirl around midspan, leading to an isolated separation on one rotor blade. The flow quickly reattaches as the blade leaves the vortex. This is a very small effect compared with the effects from the intake separation and potential field influences on the flow. This is partly due to the short length scale

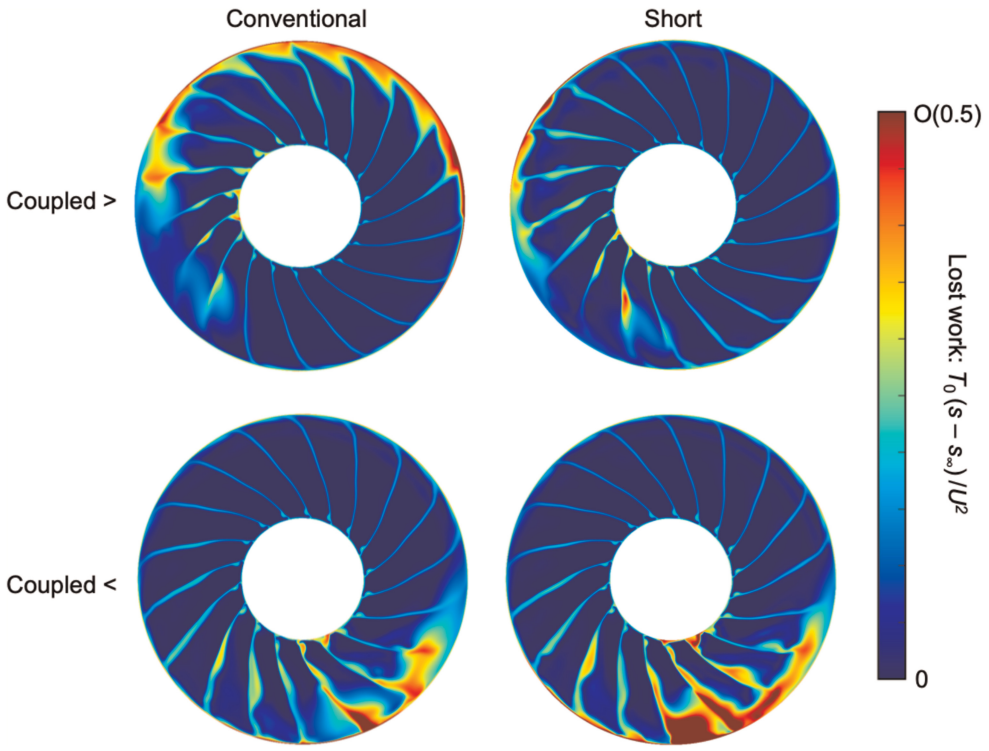

Figure 11. Contours of instantaneous lost work at rotor exit for crosswind cases.

of the ground vortex and partly because it is acting to reduce the tip incidence, which somewhat alleviates the effect of the blades entering the intake separation. It is better for the ground vortex to raise the incidence near midspan where the blades are otherwise unaffected.

For flow from the left onto the conventional intake, the fan inlet flow field and loss were found to vary unsteadily. Of the four cases tested, this was the only one where significant unsteadiness occurred. It will be shown below that this case has the highest average fan loss so it is possible that this case is brought closest to stall

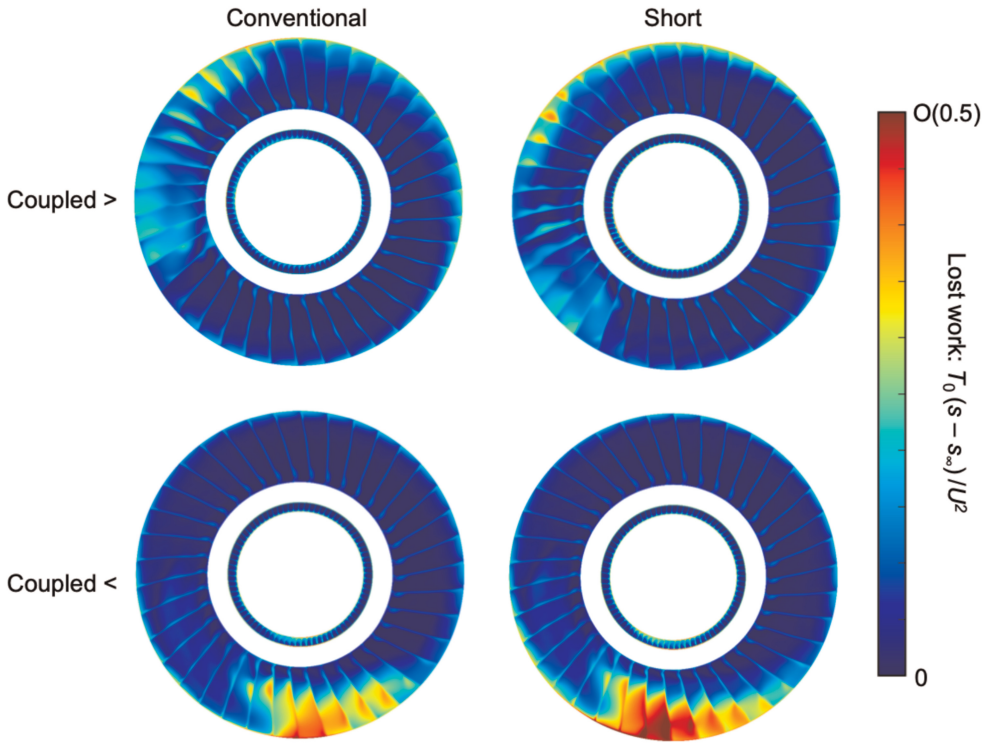

Figure 12. Contours of time-averaged lost work at stage exit for crosswind cases.

and the unsteady fan-intake interaction is indicative of an almost-stalling behavior, which has been observed in real engine tests (Freeman and Rowe, 1999).

Referring to Figure 12 the OGV is affected by further flow separations near the casing, downstream of the corresponding separations in the rotor. An additional area is affected by the upstream ground vortex. Wherever the ground vortex is co-swirling the rotor work input is reduced, lowering the OGV inlet stagnation pressure. The resulting low energy flow separates in a group of blades downstream of the vortex. This effect is similar in both intakes. The ESS is relatively unaffected for this freestream flow direction, as the rotor loss and ground vortex influences tend to remain confined to the casing, but does experience regions of increased corner separation size which lie downstream of enlarged rotor hub corner separations (Figure 11).

Flow from the right

For flow from the right, the ground vortex acts to increase the tip incidence and is located near the intake separation. Its effect merges with that of the separation, making the rotor flow separations larger and tending to form corner separations extending down the span.

In this case it is the short intake that leads to larger flow separations in the fan, although the difference between the two intakes is smaller than it was for a left-side separation. Figures 9 and 10 show that outside the separation, the short intake has stronger counter-swirl and greater positive incidence in this region. This increases the loading elsewhere on the blade, allowing the separations to grow larger.

This is essentially the opposite of the beneficial co-swirl effect created by the short intake for freestream flow from the left. This observation helps to explain the performance results in the next section, where the short intake leads to better fan rotor performance than the conventional intake for flow from the left, but worse performance for flow from the right.

The impact on the OGV (Figure 12) is also more severe for this freestream direction and this is largely a secondary consequence of the increased rotor loss. A large group of separations is present at the bottom of the annulus for both intakes, immediately downstream of the large rotor tip separations. Again, for this flow direction the ground vortex influence on the loss merges with the influence of the intake separation so the OGV separations are grouped into one area instead of being split. The ESS is affected in the same way due to the presence of large rotor hub corner separations (Figure 11).

Performance

Figures 13 to 15 break down the overall effect on stage performance. Pressure ratio and mass flow rate are reduced compared to their clean-flow values on the working line. However, the mass flow rate remains well above the stalling value. The finding is that there is a steady reduction in thrust rather than full instability.

At this separated crosswind condition, there is little difference between conventional and short intakes in overall full stage performance. It was shown above that in both intakes the flow separates in a similar way at a similar location: shock-driven separation from the highlight. At severe crosswind conditions, the intake can be assumed to be separated. If the separation mechanism is similar in both intake designs, it is to be expected that the impact on the fan will in turn be similar in both cases.

The fan work input is significantly lower when the freestream flows from the left. This effect is large enough that the fan has lower stage pressure ratio for flow from the left than from the right, even though the latter is actually the condition with higher fan loss (c.f. Figures 13 and 15). This is mainly caused by the change in sense of the ground vortex rotation relative to the fan. For freestream flow from the left, the vortex is co-rotating with the rotor, creating an average co-swirl at rotor inlet, and vice-versa. This is superimposed on an ever-present bulk swirl pattern due to flow redistribution, but this component of swirl is irrotational so it does not affect the average rotor work.

Due to the summations of these work and loss effects, the full stage performance shows little bottom-line difference between the two directions of freestream flow. However, this belies the fact that there are considerable differences in the detailed flow field, fan loss sources, overall fan loss and fan work input. It is therefore possible that the different crosswind directions lead to different remaining amounts of stability margin at this condition. This has not been tested here but would be an important consideration and motivates a full assessment of the stability range. It is also possible that different fan designs would react to in a different way; the work input effect depends on the ground vortex but the loss effect is likely to be more sensitive to fan design. It is therefore important to consider these results in the context of the detailed flow field, not just the 1D numbers.

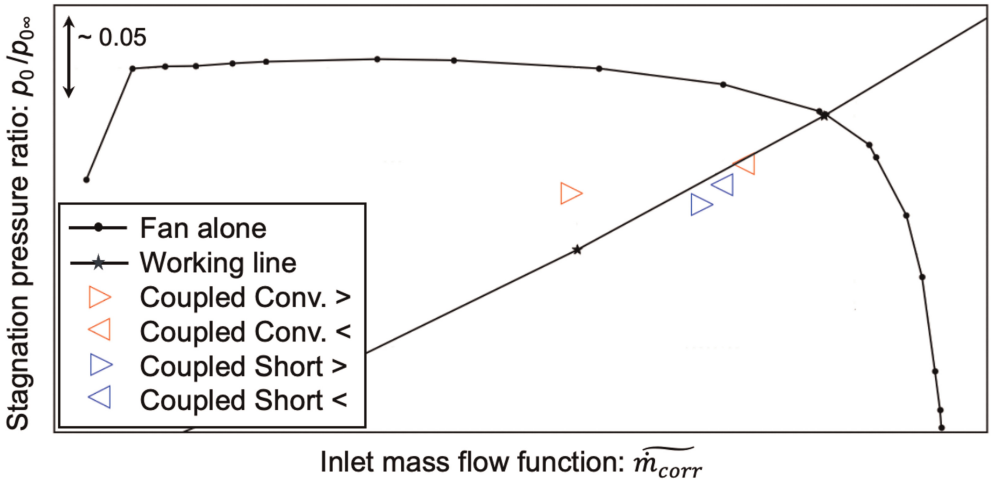

(a) Rotor

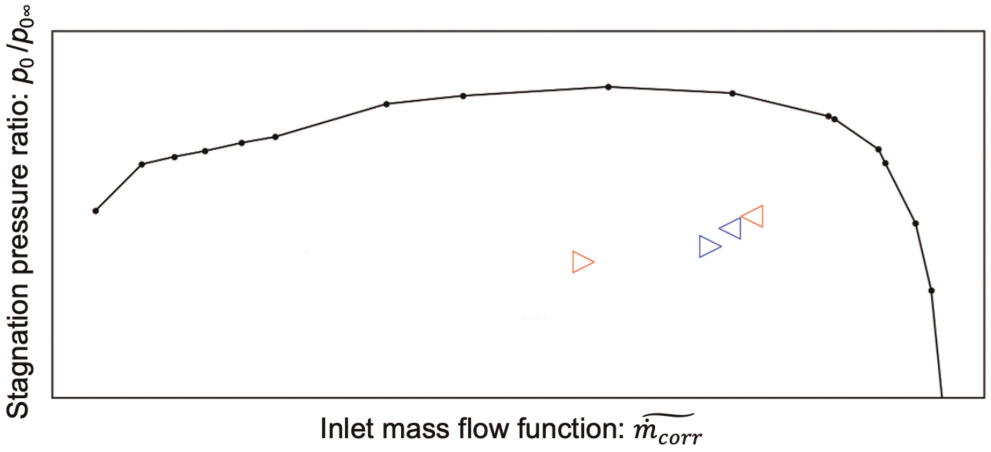

(b) Full stage including intake, rotor, OGV and ESS

Figure 13. Time-averaged rotor and full stage total pressure ratio for steady rig-alone and unsteady coupled calculations. Full stage values include the intake, rotor and a mass average of the bypass and core streams.

The rotor is the single most severely affected component in terms of loss generation. Nevertheless every component is affected and the stator loss should not be neglected. The loss incurred in the intake itself due to the flow separation is higher for the conventional intake than the short intake due to the additional distance available for mixing before the fan redistributes the separated flow.

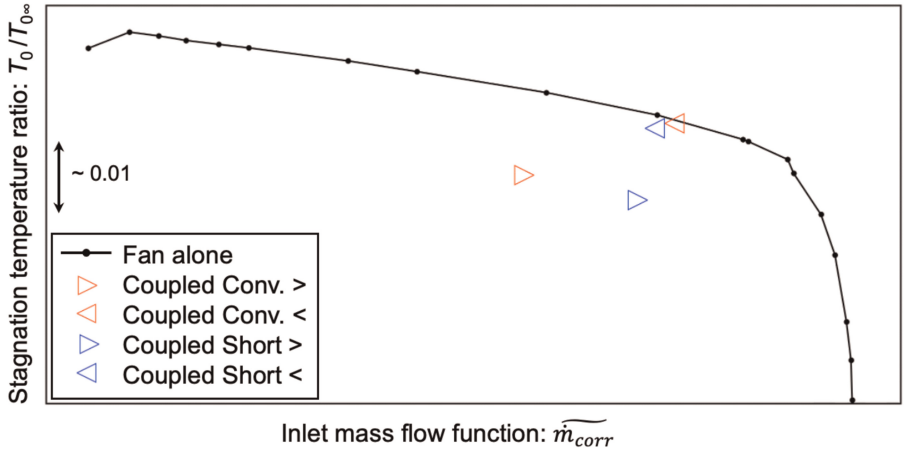

Figure 14. Time-averaged rotor total temperature ratio for steady and unsteady coupled calculations.

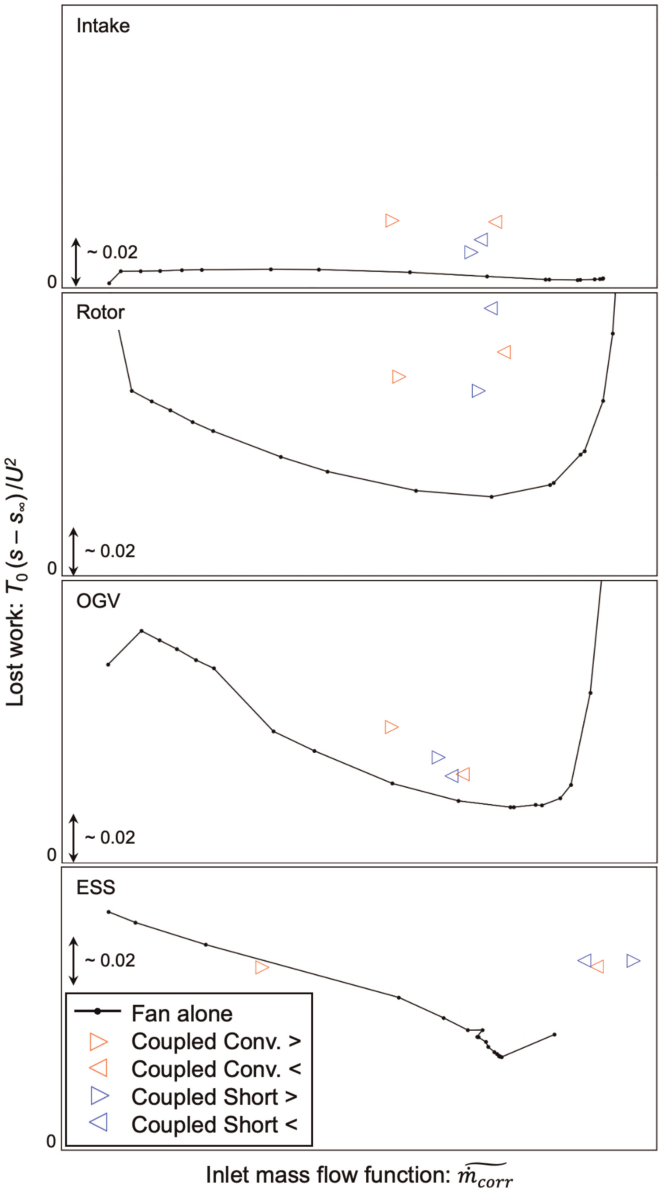

Figure 15. Time-averaged intake, rotor, OGV and ESS lost work for steady rig- alone and coupled unsteady calculations. All plots have the same vertical axis range such that they show a true loss breakdown.

Conclusions

1. The flow field at crosswind depends on multiple features including the freestream momentum and direction, intake droop, ground vortex and fan aerodynamic response. The equilibrium flow field can only be determined by coupled unsteady CFD of the fan, intake and external domain.
2. The local combination of total pressure and swirl distortion drives the response of the fan in terms of work and loss.
3. For crosswind from the left (looking into the engine with a clockwise rotating fan) the ingested ground vortex is co-rotating and reduces the fan work. For crosswind from the right, the ground vortex is counter-rotating, which increases the incidence as the fan leaves the windward lip separation. This leads to higher work and casing separations with greater spanwise extent.
4. A short intake has a more aggressive diffuser reducing the ability of any separated flow to reattach before reaching the fan. The variation of swirl at the fan face is also greater with a short intake, which contributes to a stronger separation for crosswind from the right. However, for a short intake the close coupling of the fan and intake suppresses separation and reduces the loss for crosswind from the left.
5. Despite the severe fan-distortion interaction, this paper has shown for both short and conventional intakes the low pressure ratio fan considered can operate stably in strong crosswinds without a significant drop in performance.

6. The physics of the fan-distortion interaction with crosswind can be applied to other fan and intake designs. For example, in the case of an anticlockwise rotating fan, crosswind from the left will lead to a high work and high loss configuration. However, the detailed impact of a different design on the flow-field is unknown and would require further study.

Nomenclature

Roman symbols

A	Area
D_F	Fan diameter
h	Enthalpy, intake ground clearance
i	Incidence angle
L	Intake length measured from fan leading edge
M	Mach number
$\dot{m}, \dot{m}_{corr}$	Mass flow rate, Corrected mass flow rate
p	Pressure
PR_{yx}	Pressure ratio $= p_{0y}/p_{0x}$
r	Radius, Radial coordinate
s	Entropy
T	Temperature
U	Rotor tip blade speed
V	Velocity

Greek letters

α	Swirl flow angle (positive in direction of fan rotation)
β	Relative swirl flow angle, Engine yaw angle
θ	Circumferential coordinate
ρ	Density
Ω	Fan rotational speed
$\widetilde{\Omega}$	Normalised fan rotational speed $= \Omega/\Omega_{Datum}$

Superscripts and subscripts

∞	Value far upstream
θ	Circumferential component
x	Axial component
0	Stagnation quantity
ref	35 kt headwind case
rel	Relative reference frame quantity

Acronyms

CFD	Computational fluid dynamics
CGI	Grid convergence index
ESS	Engine section stator
GPU	Graphics processing unit
MFCR	Mass flow capture ratio
OGV	Outlet guide vane
UHBPR	Ultra-high bypass ratio

Acknowledgments

The authors are grateful for the comments and suggestions of colleagues at the Whittle Laboratory, Rolls-Royce plc. and Imperial College, in particular Ben Mohankumar, Mark Wilson, and Nicholas Cumpsty.

Competing interests

Alejandro Castillo Pardo declares that he has no conflict of interest. Ewan Gunn declares that he has no conflict of interest. Tim S. Williams declares that he has no conflict of interest. Cesare Hall declares that he has no conflict of interest. Tobias Brandvik declares that he has no conflict of interest. Stephane Baralon declares that he has no conflict of interest.

Funding sources

Innovate UK under project reference 113286: FANFARE.

References

Allen O., Castillo Pardo A., and Hall C. A. (2021). An experimental investigation into the impacts of varying the circumferential extent of tip-low total pressure distortion on fan stability. In: Proceedings of the ASME Turbo Expo 2021, Vol. 84904. American Society of Mechanical Engineers. p. V02AT31A036.

Brandvik T. and Pullan G. (2011). An accelerated 3D Navier-Stokes solver for flows in turbomachines. *Journal of Turbomachinery*. 133 (2): 021025. https://doi.org/10.1115/GT2009-60052.

Castillo Pardo A., Mehdi A., Pachidis V., and MacManus D. G. (2014). Numerical study of the effect of multiple tightly-wound vortices on a transonic fan stage performance. In: Proceedings of the ASME Turbo Expo 2014, number GT2014-26481. American Society of Mechanical Engineers.

Celik I. B., Ghia U., Roache P. J., and Freitas C. J. (2008). Procedure for estimation and reporting of uncertainty due to discretization in CFD applications. *Journal of Fluids Engineering*. 130 (7): 078001. https://doi.org/10.1115/1.2960953.

De Siervi F., Viguier H. C., Greitzer E. M., and Tan C. (1982). Mechanisms of inlet-vortex formation. *Journal of Fluid Mechanics*. 124: 173–207. https://doi.org/10.1017/S0022112082002456.

Freeman C. and Rowe A. (1999). Intake engine interactions of a modern large turbofan engine. In: Proceedings of ASME 1999 International Gas Turbine and Aeroengine Congress and Exhibition, number 99-GT-344. American Society of Mechanical Engineers.

Hoheisel H. (1997). Aerodynamic aspects of engine-aircraft integration of transport aircraft. *Aerospace Science and Technology*. 1 (7): 475–487. https://doi.org/10.1016/S1270-9638(97)90009-2.

Jameson A. (1991). Time dependent calculations using multigrid, with applications to unsteady flows past airfoils and wings. In: AIAA 10th Computational Fluid Dynamics Conference. American Institute of Aeronautics and Astronautics. p. 1596.

Kim S., Pullan G., Hall C. A., Grewe R. P., Wilson M. J. et al. (2019). Stall inception in low-pressure ratio fans. *Journal of Turbomachinery*. 141 (7): 071005. https://doi.org/10.1115/1.4042731.

Lee K., Dodds J., Wilson M., and Vahdati M. (2018). Validation of a numerical model for predicting stalled flows in a low-speed fan - part ii: unsteady analysis. *Journal of Turbomachinery*. 140 (5): 051009. https://doi.org/10.1115/1.4039052.

Liu Y., Lu L., Fang L., and Gao F. (2011). Modification of Spalart–Allmaras model with consideration of turbulence energy backscatter using velocity helicity. *Physics Letters A*. 375 (24): 2377–2381. https://doi.org/10.1016/j.physleta.2011.05.023.

Mohankumar B., Hall C. A., and Wilson M. J. (2021). Fan aerodynamics with a short intake at high angle of attack. *Journal of Turbomachinery*. 143 (5): 051003. https://doi.org/10.1115/1.4050606.

Murphy J. P. and MacManus D. G. (2011). Ground vortex aerodynamics under crosswind conditions. *Experiments in Fluids*. 50 (1): 109–124. https://doi.org/10.1007/s00348-010-0902-4.

NUMECA International (2016). Autogrid5. Accessed 13 July 2018. http://www.numeca.com/product/autogrid5.

Pointwise Inc (2023). Pointwise. Accessed 23 January 2023. http://www.pointwise.com/index.html.

Spalart P. R. and Allmaras S. (1992). A one-equation turbulence model for aerodynamic flows. In: Proceedings of the 30th Aerospace Sciences Meeting and Exhibit. American Institute of Aeronautics and Astronautics. p. 439.

Trapp L. G. and da Motta Girardi R. (2010). Crosswind effects on engine inlets: the inlet vortex. *Journal of Aircraft*. 47 (2): 577–590. https://doi.org/10.2514/1.45743.

Williams T. S., Hall C. A., and Wilson M. J. (2020). Low pressure ratio transonic fan stall with radial distortion. *Journal of the Global Power and Propulsion Society*. 4: 226–237. https://doi.org/10.33737/jgpps/130478.